Multisection Cerebral Blood Flow MR Imaging with Continuous Arterial Spin Labeling

Multisection Cerebral Blood Flow MR Imaging with Continuous Arterial Spin Labeling[1]

David C. Alsop, PhD
John A. Detre, MD

Index terms:
Cerebral blood vessels, flow dynamics
Cerebral blood vessels, MR, 17.121413, 17.121419
Magnetic resonance (MR), echo planar, 17.121419
Magnetic resonance (MR), vascular studies, 17.121419

Radiology 1998; 208:410–416

Abbreviations:
CBF = cerebral blood flow
RF = radio frequency

[1] From the Departments of Radiology (D.C.A., J.A.D.) and Neurology (J.A.D.), University of Pennsylvania Medical Center, 3400 Spruce St, Philadelphia, PA 19104-4283. Received September 3, 1997; revision requested November 19; revision received February 27, 1998; accepted April 10. Supported in part by National Institutes of Health grants P30-MG93880 and P50-NS08803. D.C.A. supported in part by a Biomedical Engineering Research Grant from the Whitaker Foundation. J.A.D. supported in part by the National Institutes of Health grant NS01668. **Address reprint requests to** D.C.A.

See also the editorial by Jezzard (pp 296–299) in this issue.

Author contributions:
Guarantor of integrity of entire study, D.C.A.; study concepts and design, D.C.A., J.A.D.; definition of intellectual content, D.C.A., J.A.D.; literature research, D.C.A., J.A.D.; experimental studies, D.C.A., J.A.D.; data acquisition, D.C.A., J.A.D.; data analysis, D.C.A.; statistical analysis, D.C.A.; manuscript preparation, D.C.A.; manuscript editing, D.C.A., J.A.D.

A method was evaluated to control for off-resonance saturation in noninvasive magnetic resonance imaging with continuous arterial spin labeling of cerebral blood flow. In phantoms and humans, application of amplitude-modulated radio-frequency irradiation during the control image corrected for saturation across the whole brain and made possible cerebral blood flow imaging in multiple sections at arbitrary angles to the labeling plane.

Measurement of regional cerebral blood flow (CBF) provides useful information about both cerebrovascular sufficiency and regional brain metabolism because resting CBF and tissue metabolism are often strongly coupled (1). CBF imaging with single photon emission computed tomography (CT), or SPECT, positron emission tomography, or PET, and xenon-enhanced CT have been used to evaluate a multitude of cerebral disorders including stroke (2), dementia (3), epilepsy (4), trauma (5), and neoplasms (6). Positron emission tomography of CBF has also been an important tool for mapping task-induced brain activity in normal and pathologic states (7). For most central nervous system disorders, magnetic resonance (MR) imaging provides the greatest sensitivity to structural abnormalities. A robust MR imaging–based method for clinical imaging of CBF would allow both an anatomic and a functional assessment within the same examination. In addition to providing direct structure-function correlation, the higher spatial resolution of MR imaging compared with that of nuclear medicine methods might also lead to better image quality. MR imaging of CBF can be performed with either intravascular contrast agents (8,9) or arterial spin labeling (10,11). Instead of using an exogenous tracer, arterial spin labeling electromagnetically labels water proton spins in the feeding arteries before they flow into the tissue. Arterial spin labeling is attractive because it can help reduce the risk, complexity, and cost of a study. It is also more readily quantified and repeated than methods that involve use of contrast agents.

Arterial spin labeling techniques can be crudely divided into pulsed inversion techniques (eg, echo-planar imaging and signal targeting with alternating radio frequency, or EPISTAR [12]; flow-sensitive alternating inversion recovery, or FAIR [13,14]; and other variants) and techniques that employ continuous arterial spin labeling (11). Continuous arterial spin labeling produces more than twice the signal of pulsed inversion techniques (15). With both methods, multisection imaging is complicated by the effects of electromagnetic labeling on the signal intensity, as well as the relatively long time required for blood to flow from the arteries into the thick slab of tissue to be imaged.

The arterial spin labeling approach to MR imaging of CBF offers the potential for completely noninvasive, quantitative imaging of an important physiologic and diagnostic quantity. Practical implementations of arterial spin labeling in humans, however, have typically suffered from systematic errors and artifacts that have limited its applicability. Recently, the use of fast imaging methods and an increased understanding of the factors affecting quantification of CBF have led to the acquisition of single-section CBF images with sufficiently high quality to allow clinical and research applications to be explored (12,15,16). Unfortunately, most applications require greater section coverage, but the serial acquisition of

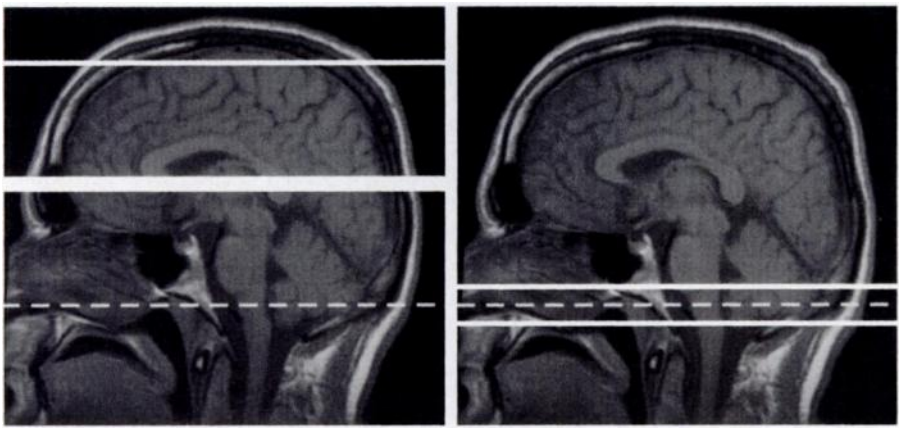

a. b.

Figure 1. Control methods for CBF imaging with continuous arterial spin labeling illustrated on sagittal T1-weighted spin-echo images. RF irradiation used to label inflowing blood as it crosses the labeling plane (dashed line in **a** and **b**) also causes direct effects on image intensity that vary with distance from the labeling plane. **(a)** In the single-section experiment, the control image is acquired with labeling (thin solid line) applied at an equal distance distal to the imaged section (thick solid line) to compensate for the spatially dependent off-resonance effects. **(b)** In the multisection experiment, amplitude-modulated irradiation applied for the control image creates two inversion planes (solid lines) close to the original labeling plane. Ideally, the inflowing spins are inverted twice as they flow through the planes, producing no net effect on arterial labeling, while the spatially dependent off-resonance effects of the RF irradiation are precisely reproduced.

many sections can be prohibitively time-consuming. Improved radio-frequency (RF) pulse shapes and sequence designs may make multisection pulsed arterial spin labeling techniques feasible (17). In this study, we evaluated a method for multisection imaging with continuous arterial spin labeling in which amplitude-modulated RF irradiation was used to control for the off-resonance effects of labeling. This method makes possible multisection imaging of CBF with good signal-to-noise ratio and arbitrary angles between imaging and labeling planes.

Materials and Methods

Amplitude-modulated Control

Continuous application of off-resonance RF power causes saturation of signal intensity as a result of the finite width of the water line and the transfer of saturated magnetization from water molecules adjacent to macromolecules, which have much broader lines (18). The off-resonance inversion power applied in continuous arterial spin labeling usually causes such saturation, and its presence complicates CBF imaging because the off-resonance effects may be large compared with the effects of blood flow. An approach to eliminating this saturation is the use of a second small RF coil for labeling that is far enough from the imaged section that the off-resonance power is negligible. This method has been used successfully to obtain multisection CBF images in rat brain (19), but it requires use of special RF hardware and a favorable geometry for the labeling, which limit its applicability. The alternative is to control for the saturation. Because CBF imaging with arterial spin labeling relies on the subtraction of the labeled image from a reference image obtained without labeling, achievement of equal off-resonance saturation in the reference image will control for the saturation effect.

The established method of controlling for off-resonance saturation with a single RF coil (11) is to apply an inversion distal to the section during acquisition of the control image (Fig 1a). If there are no noticeable background magnetic field gradients in the tissue, the off-resonance saturation is symmetric in frequency, and the labeling and control inversion are parallel to and equidistant from the image section, then the control image will experience equal off-resonance saturation. The requirement that the labeling and control inversion planes be parallel to and equidistant from the image section restricts the geometry of CBF imaging with arterial spin labeling and is not readily extended to use in a multisection examination. To overcome these limitations, use of an alternative control irradiation that mimics the frequency-dependent off-resonance effects of the labeling irradiation is required.

In this study, we evaluated application of an amplitude-modulated form of the labeling RF irradiation for the control. When a constant RF irradiation at a fixed frequency, f_0, is multiplied by a sine wave at frequency f_1, the signal produced is mathematically identical to continuous irradiation at two different frequencies, $f_0 + f_1$ and $f_0 - f_1$. If applied in the presence of a magnetic field gradient, each would separately perform an adiabatic inversion of inflowing arterial spins. When performed simultaneously, the combined effect is complicated because the equations governing spin evolution are not linear in the applied RF. However, the nature of resonance suggests that the effect of the first inversion on spins located near the plane of the second inversion should be small as long as the frequency spacing between the planes is large. In this case, the spins will be inverted twice after flowing through the two inversion planes (Fig 1b). Double inversion produces no net effect, so spins would not be labeled by the amplitude-modulated control. Because the average power and center frequency of the amplitude-modulated control are identical to those of the labeling RF irradiation, we hypothesized that the off-resonance effects of the control would be nearly identical to those of the labeling.

The performance of amplitude modulation of the RF irradiation as a control will depend on how perfectly the spins are doubly inverted, as well as on how well the off-resonance saturation of the labeling irradiation is matched. If the spins are partially labeled by the amplitude-modulated control, then the difference between the labeled and control images will decrease. This can be thought of as a loss of efficiency for labeling of blood flow. If the control does not perfectly match the off-resonance saturation of the labeling, then a difference between the images will occur even in the absence of blood flow. This would represent a systematic error in the blood flow measurement. We assessed both of these properties of the control experimentally.

MR Imaging

All studies were performed on a 1.5-T clinical imager (Signa; GE Medical Systems, Milwaukee, Wis) equipped with a prototypic gradient system for echo-planar imaging. Gradient-echo echo-planar images were obtained with a field of view of 24 (frequency) × 15 (phase) cm and an acquisition matrix of 64 × 40. Acquisition bandwidth of ±62.5 kHz al-

lowed an effective echo time of 22 msec and an image acquisition time of 45 msec. Multisection image acquisition was performed without pausing between sections; therefore, eight sections could be acquired in less than 400 msec. Section thickness was 6–10 mm and intersection gaps were 2 mm to minimize potential interference between sections.

Spin labeling was performed as previously reported for single-section CBF imaging (15) except for the amplitude-modulated control and the acquisition of more than one section. Specifically, a repetition time of 4,000 msec, temporal interleaving of labeled and control images, and a postlabeling delay were employed. The postlabeling delay reduces the sensitivity of the CBF image to the transit time from the labeling plane, attenuates the signal from intraluminal arterial spins, and decreases the off-resonance saturation of the signal intensity by the labeling RF (15). The postlabeling delay also allows time for all of the labeled blood to enter the tissue before imaging so that saturation of labeled spins by the imaging excitation pulses need not be considered. The duration of the labeling irradiation was determined on the basis of the postlabeling delay, the imaging time, and the repetition time. For a postlabeling delay of 1.2 seconds, the irradiation was applied for 2.3 seconds. A timing diagram for the entire sequence is shown in Figure 2.

Multisection versions of previously described echo-planar T1 mapping images (15) were obtained in addition to the CBF image. The T1 maps are needed to quantify the CBF images. Unlike in the single-section implementation, the labeling gradient had to be left on during T1 mapping to accurately measure the T1 shortening effect of the off-resonance saturation. In all other ways, the protocol was identical. The entire T1 mapping protocol required 3 minutes for all sections.

All raw echo amplitudes were saved and transferred to a workstation for processing. Custom software written within the Instructive Data Language (IDL; Research Systems, Boulder, Co) environment was used to reconstruct the images. Correction for image distortion and alternate k-space line errors was performed on each image on the basis of data acquired during phase-encoded reference imaging (20). Correction for distortion involves measurement of magnetic field nonuniformity throughout the image. A side effect of this correction is that image regions are set to zero in which insufficient MR signal is present to allow accurate measurement of the magnetic field. Magnitude images were then averaged, and CBF-weighted images were calculated by subtracting labeled images from control images. An algorithm to remove subtle motion artifacts from the images (21) was performed on the individual images before averaging to allow more accurate evaluation of the performance of the control.

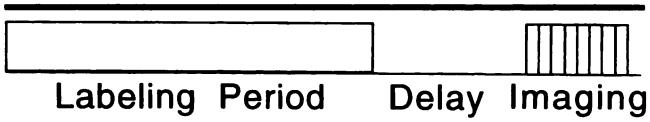

Figure 2. Pulse sequence timing diagram. Labeling RF and gradients are applied during the labeling period. A postlabeling delay is inserted between labeling and imaging to provide insensitivity to transit time. Finally, rapid gradient-echo echo-planar imaging is performed to acquire images in eight sections.

Phantom Studies

Before evaluation in human subjects, the sequence was tested and calibrated on a uniform phantom consisting of 2% agarose by weight in distilled H_2O. Use of a phantom with noticeable magnetization transfer was necessary to fully test the control. The magnetization transfer properties of agarose are well studied (22), but they are considerably different from those of most human tissues (23). We hoped that the control would be accurate across a wide range of tissue types and that the agarose phantom would serve as an extreme case. The phantom consisted of a cylindric plastic container, 10 cm in diameter and 20 cm long, filled with the gelatinous mixture. The phantom was placed in the standard head coil of the imager with its axis parallel to that of the magnet. Single-section images obtained with the CBF labeling strategy were acquired in a plane perpendicular to the axis of the phantom. Labeling RF irradiation of 35 mG and a labeling gradient of 0.25 G/cm applied along the frequency direction of the image were used. Images were acquired with amplitude modulation frequencies of 125, 250, and 500 Hz. Off-resonance saturation was analyzed by averaging the images across the phase direction so that plots of off-resonance saturation as a function of frequency could be generated.

During evaluation of the sequence, we found that weak saturation of signal at the labeling plane occurred even when the RF amplitude was set to zero in the software. This indicated that a small amount of RF was leaking past the modulator. The saturation could be eliminated by setting the RF amplitude to a small negative value corresponding to 2% of the RF amplitude used for labeling. A constant value of 2% of the labeling amplitude was subtracted from the software values of all labeling-related RF amplitudes to compensate for this carrier leakage. Failure to correct for this leakage causes systematic error in the CBF measurement. Because the leakage is a subject-independent phenomenon, it can be calibrated with phantom measurements and need never be measured in subjects. The leakage on our imager has remained stable for more than 1 year.

Human Studies

All human studies were conducted on the basis of a protocol approved by our institutional review board. Written informed consent was obtained from 11 healthy volunteers. Three different studies were performed.

In one study, the amplitude-modulated control method was tested for systematic offset due to imperfect matching of the off-resonance saturation for label and control. Two subjects underwent MR imaging with control modulation frequency of 250 Hz, RF irradiation amplitude of 35 mG, postlabeling delay of 1.2 seconds, and 0.25 G/cm labeling gradient. Images of eight 8-mm-thick sections were obtained in both subjects when the labeling was applied to the carotid and vertebral arteries at the pontomedullary junction, to generate CBF images, and also when the labeling was applied distal to the imaging section at the top of the brain, which should produce no flow-related signal intensity in the absence of systematic error. One of the subjects underwent axial MR imaging and the other underwent coronal MR imaging to emphasize the flexibility of section geometry possible with use of amplitude-modulated control.

In a second study, the efficiency of multisection versus single-section CBF measurement was compared. In nine sub-

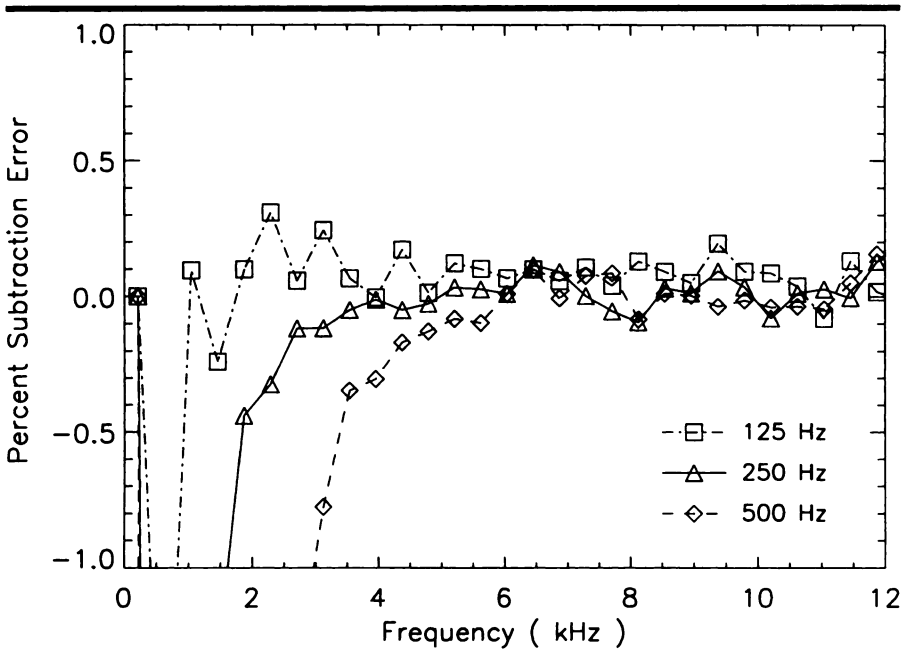

Figure 3. Graph depicts percentage difference between labeled and control images of the phantom as a function of frequency. Results for three different amplitude-modulation frequencies are shown.

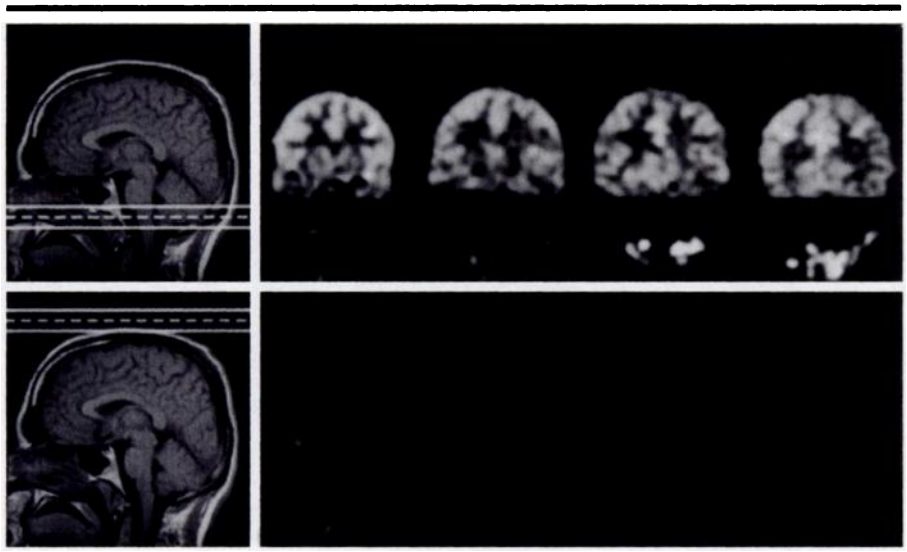

Figure 4. Evaluation of the amplitude-modulated control in a healthy subject. Left: Coronal echo-planar images (4,000/22 [effective]) were acquired with label and control placed at the pontomedullary junction (top) and above the brain (bottom) as indicated on the sagittal T1-weighted images. Right: Multisection subtraction images acquired with proximal labeling (top) demonstrate signal intensity from CBF. Images acquired with distal labeling (bottom) show no noticeable signal intensity.

jects, CBF images were acquired in a single axial section through the basal ganglia and thalamus. Images were acquired with both the single-section method, in which control labeling is distal to the section, and the multisection method. All subjects were studied with 0.25 G/cm labeling gradient, RF irradiation amplitude of 35 mG, control modulation frequency of 250 Hz, postlabeling delay of 1.2 seconds, and labeling plane offset of 4–8 cm from the section. From 15 to 45 pairs of labeled and control images were obtained in each subject for every combination of experimental parameters. In three of these subjects, the single-section and multisection methods were also compared at RF amplitudes of 30 and 20 mG. In three other subjects, the methods were also compared with modulation frequencies of 62.5, 100, 125, 200, and 500 Hz.

In the final human study in four subjects, multisection CBF images and T1 maps were obtained with 250-Hz modulation and 35-mG RF amplitude for quantitative analysis of CBF with use of previously presented methods (15). The entire CBF imaging sequence required 9 minutes including T1 mapping and acquisition of 45 pairs of labeled and control images. The efficiency value for multisection labeling measured in the first study was used for quantification.

Results

Phantom Study

Matching of frequency-dependent off-resonance saturation effects between the labeling and amplitude-modulated control was excellent at all three frequencies, as shown in Figure 3. Though both types of irradiation produced off-resonance saturation of greater than 15% of the unsaturated signal, the difference between the two was less than 0.1% except very close to the labeling plane. The frequency at which the difference between the labeled and control frequencies became noticeable was smaller for amplitude modulation at lower frequency. This suggests that labeling can be performed closer to the most inferior region to be imaged when slower amplitude modulation is used.

Human Studies

Excellent matching between the labeling and control off-resonance saturation in the phantom was also reproduced in the in vivo studies. Figure 4 shows the coronal subtracted images obtained with labeling 2 cm above the top of the brain and at the pontomedullary junction. The images with the pontomedullary junction label show strong CBF signal intensity in all distal regions of the brain, but those with the label above the brain show no noticeable signal intensity. To further quantify residual subtraction errors caused by imperfect matching of off-resonance saturation, the signal intensity was averaged across the section and phase directions, similar to the phantom analysis, and the results are plotted in Figure 5. CBF produces a signal intensity change of less than 1% on the proximal labeled images, whereas residual subtraction error for frequencies above 2 kHz as mea-

sured on the distal labeled images is consistent with noise and is always less than 0.05%. The average of the subtracted signal intensity across frequency from 2 to 10 kHz is less than 0.007% of the control signal intensity. Because the CBF images were acquired in a plane perpendicular to the labeling plane, their uniformity is also a direct indicator of the accuracy of the control. Errors in subtraction are apparent in the perfusion signal intensity (Fig 5) very near the labeling plane at offset frequencies below 2 kHz. The subtraction error produces a shift to a negative signal intensity; this finding is consistent with the phantom results (Fig 3). A comparable level of matching was observed on axial images acquired in another subject (not shown).

The mean efficiency ratio of the multisection and single-section methods was 61.6% ± 6.7 (standard deviation) across the nine subjects with a modulation frequency of 250 Hz. This efficiency was found to drop rapidly when the RF amplitude was lowered; efficiency at 30 mG was 58% and at 20 mG was only 35%. The efficiency at 36-mG amplitude improved to 75% when the modulation frequency was lowered (Fig 6). This suggests that a modulation frequency of 62.5 Hz is more desirable than 250 Hz.

Quantification of the CBF images was performed with use of methods described previously for single-section imaging. The averaged labeled images were first subtracted from the averaged control images and then divided by the signal intensity on an image obtained in the absence of off-resonance saturation. This ratio was then multiplied by a calibration factor (Eq [9] in reference 15), which is a function of the calculated T1 images, the transit times to the tissue from the labeling plane, and the postlabeling delay for each section. Because the transit time to the tissue was not measured, an assumed value of 1.5 seconds was employed for quantification. The long postlabeling delay minimized sensitivity of the calibration factor to differences between the assumed and actual transit times. Images were corrected for inefficiency of labeling by dividing by an efficiency value of 58.5%. This value was based on an efficiency value of 95% for the single-section experiment (24) and the ratio between multisection and single-section efficiency measured in this study, 61.6%. Calculated images from one of the subjects are in Figure 7. These images are not corrected for spatial variations in the blood-brain partition coefficient. Quantitative CBF values were derived by segmenting the tissue into gray and white matter on the basis of the T1 maps and by using partition coefficients of 0.98 for gray matter and 0.82 for white matter (25). Our measured CBF values (Table) are consistent with those obtained previously with single-section methods (15,26) and with other measurements of CBF (27).

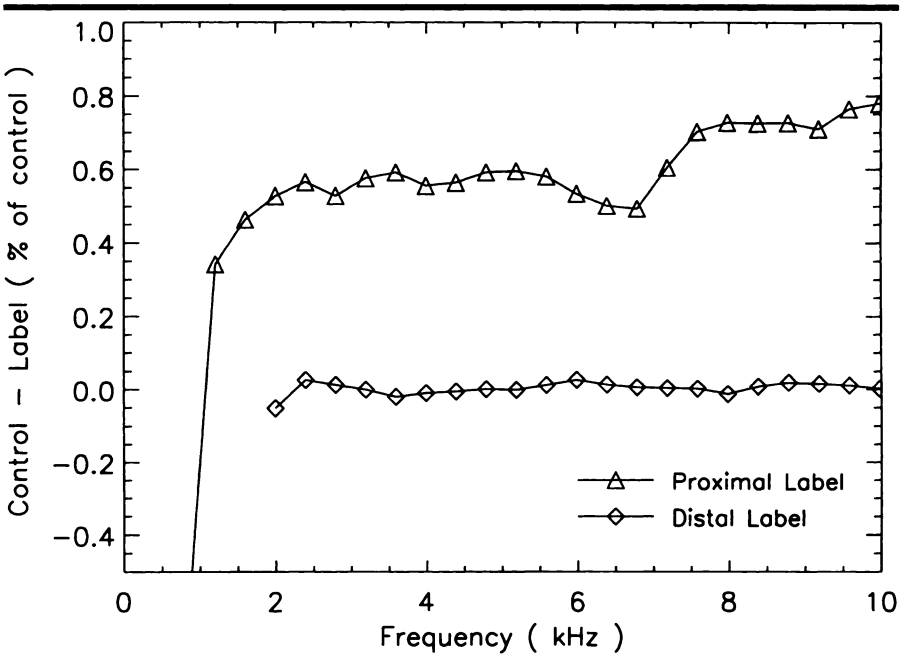

Figure 5. Graph depicts the mean difference in signal intensity obtained by averaging the images in Figure 4 across the anteroposterior and right-left directions. For plotting, distance from the labeling plane was converted into frequency offset. Proximal labeling at the pontomedullary junction produced a small but very noticeable change in the signal intensity due to CBF. Distal labeling above the brain produced no noticeable signal intensity change; this finding is consistent with negligible off-resonance errors for offset frequencies above 2 kHz.

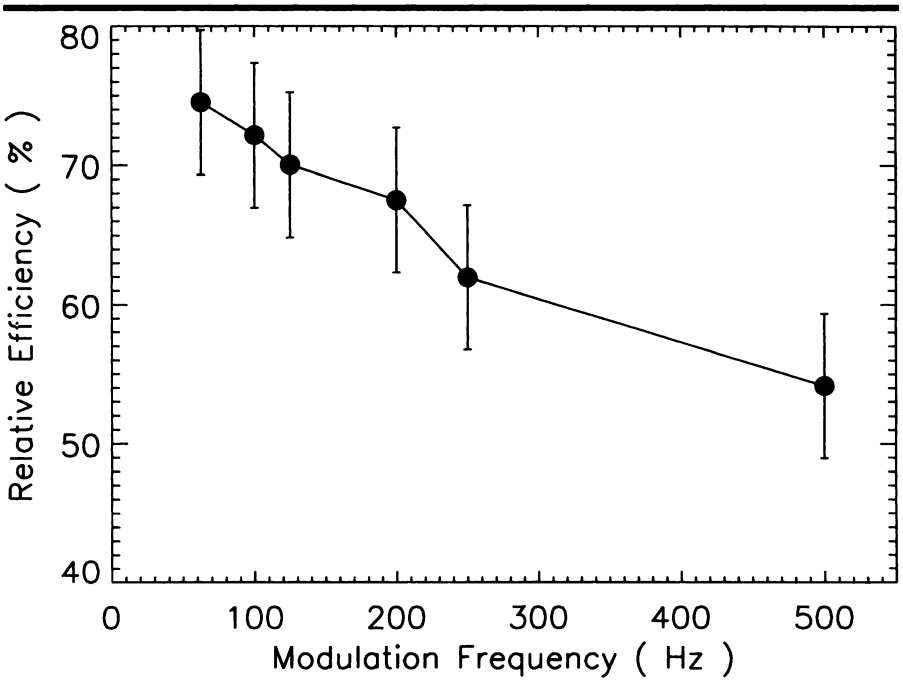

Figure 6. Graph depicts efficiency of spin labeling with the amplitude-modulated control as a function of modulation frequency relative to single-section labeling with 36-mG irradiation.

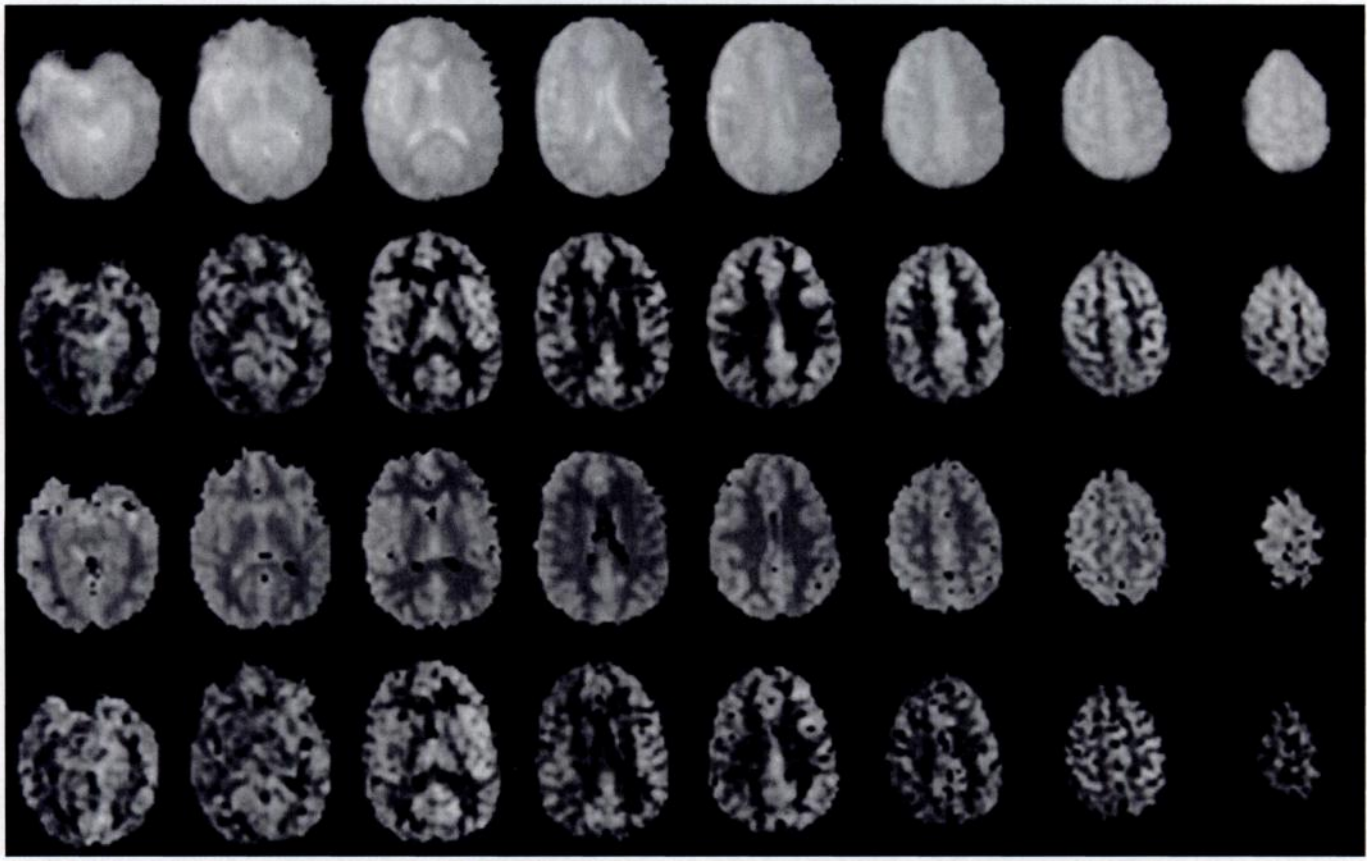

Figure 7. Multisection images acquired in a healthy volunteer. Echo-planar images (4,000/22 [effective]) from eight axial sections (top row) were used to generate CBF-sensitive images (second row). On the basis of the T1 maps (third row) also acquired, quantitative CBF images (bottom row) can be generated.

Discussion

We have presented a method for multisection CBF imaging using continuous arterial spin labeling with an amplitude-modulated control. This strategy is highly effective at controlling for off-resonance effects and efficient at doubly inverting inflowing spins, thus retaining the signal advantages of continuous versus pulsed arterial spin labeling techniques. The method is readily implemented with standard hardware, is effective in both gray and white matter, and allows flexible selection of the imaging and labeling planes. Because the control method is applied at the same location as the labeling and gives equal effect across a wide range of frequencies, there should be no errors associated with static magnetic field inhomogeneity or asymmetry in the off-resonance spectrum (28). The labeling method is therefore desirable for even single-section CBF imaging applications. This approach should also be applicable to blood flow measurements in organs other than the brain. Although these studies were carried out in eight sections, the number of sections is limited only by the image acquisition time and T1 of blood and tissue.

The highest efficiency was measured for the lowest modulation frequency in this study, 62.5 Hz. This was contrary to our initial intuition that the two inversion planes would start to interfere as they became closer. We have implemented numeric simulations of the control by using methods similar to those published for single-section labeling (24). These simulations suggest that inefficiency results primarily from nonlinear interactions between the two inversion planes rather than from T1 decay between the two planes. The simulation results did not faithfully reproduce the experimental behavior, however, so we report only the experimental results. Further study of the factors affecting efficiency, which we have already performed for the single-section method, are clearly necessary.

In this study, use of gradient-echo echo-planar imaging with a moderately long echo time caused signal loss in parts of the inferior frontal and temporal lobes because of nonuniform magnetic fields near bones and sinuses. Spin-echo echo-planar imaging was avoided because it would have increased the duration of image acquisition. Fractional k-space acquisition, which was not supported by our analysis software, could have enabled gradient-echo imaging with much shorter effective echo time or spin-echo echo-planar imaging with acquisition times comparable to or shorter than those in our sequence. If necessary for imaging speed or image quality, other methods such as interleaved echo-planar imaging (29) or rapid acquisition with relaxation enhancement, or RARE (30), might be employed as long as they do not unacceptably increase motion artifact.

Spin-labeled perfusion images clearly reflect CBF and its spatial and temporal variation, but further work is required to test and validate the quantitative values obtained with this technique. To our knowledge, validation of the technique only in rats with use of microspheres has been published (31). It is likely that such

Quantitative CBF in Four Healthy Volunteers

Subject No./ Age (y)*/ Sex	CBF (mL · 100 g^{-1} · min^{-1})		
	Gray Matter	White Matter	Mean
1/24/M	70.5	27.1	53.7
2/25/M	71.4	28.5	54.8
3/32/M	61.7	32.5	50.4
4/21/F	85.9	49.7	71.9
Mean†	72.4 ± 10	34.5 ± 10	57.7 ± 10

* Mean age, 25.5 years ± 5 (1 standard deviation).
† Data are the mean ± standard deviation.

studies will lead to refinements of the measurements and the equations for quantifying flow, but we are confident that reliable quantitative flow measurements can be obtained with the spin-labeling approach and that values obtained with the present technique are not far from correct.

The extension of CBF imaging with continuous arterial spin labeling to a multisection modality overcomes a major obstacle to clinical applications. We have already applied this approach successfully in patients with cerebrovascular disease (32). CBF measurements obtained with this approach are also likely to provide a sensitive and quantitative measurement of cerebrovascular reserve when performed in conjunction with administration of acetazolamide or CO_2 inhalation. Numerous other potential clinical applications can be envisioned, including differential diagnosis of dementing disorders and cerebral neoplasms. In addition, quantitative CBF measurements have applications in clinical and basic neuroscience, for imaging regional CBF changes during sensorimotor or cognitive tasks or after pharmacologic challenges, and for population-based studies of changes in regional CBF and metabolism.

References

1. Frackowiak RSJ, Pozzilli C, Legg NJ, et al. Regional cerebral oxygen supply and utilization in dementia. Brain 1981; 104:753–778.
2. Yudd AP, VanHeertum RL, Masdeu JC. Interventions and functional brain imaging. Semin Nucl Med 1991; 21:153–158.
3. Waldemar G. Functional brain imaging with SPECT in normal aging and dementia. Cerebrovasc Brain Metab Rev 1995; 7:89–130.
4. Spencer SS. The relative contributions of MRI, SPECT, and PET imaging in epilepsy. Epilepsia 1994; 35(suppl):S72–S89.
5. Jacobs A, Put E, Ingels M, Bossuyt A. Prospective evaluation of technetium-99m–HMPAO SPECT in mild and moderate traumatic brain injury. J Nucl Med 1994; 35:942–947.
6. Leenders KL. PET: blood flow and oxygen consumption in brain tumors. J Neurooncol 1994; 22:269–273.
7. Posner MI, Petersen SE, Fox PT, Raichle ME. Localization of cognitive operations in the human brain. Science 1988; 240: 1627–1631.
8. Belliveau JW, Rosen BR, Kantor HL, et al. Functional cerebral imaging by susceptibility contrast. Magn Reson Med 1990; 14: 538–546.
9. Ostergaard L, Sorensen AG, Kwong KK, Weisskoff RM, Gyldensted C, Rosen BR. High resolution measurement of cerebral blood flow using intravascular tracer bolus passages. II. Experimental comparison and preliminary results. Magn Reson Med 1996; 36:726–736.
10. Detre JA, Leigh JS, Williams DS, Koretsky AP. Perfusion imaging. Magn Reson Med 1992; 23:37–45.
11. Williams DS, Detre JA, Leigh JS, Koretsky AP. Magnetic resonance imaging of perfusion using spin inversion of arterial water. Proc Natl Acad Sci USA 1992; 89:212–216.
12. Edelman RR, Siewert B, Darby DG, et al. Qualitative mapping of cerebral blood flow and functional localization with echo-planar MR imaging and signal targeting with alternating radio frequency. Radiology 1994; 192:513–520.
13. Kwong KK, Chesler DA, Weisskoff RM, et al. MR perfusion studies with T1-weighted echo planar imaging. Magn Reson Med 1995; 34:878–887.
14. Kim SG. Quantification of relative cerebral blood flow change by flow-sensitive alternating inversion recovery (FAIR) technique: application to functional mapping. Magn Reson Med 1995; 34:293–301.
15. Alsop DC, Detre JA. Reduced transit-time sensitivity in non-invasive magnetic resonance imaging of human cerebral blood flow. J Cereb Blood Flow Metab 1996; 16:1236–1249.
16. Buxton RB, Frank LR, Siewert B, Warach S, Edelman RR. A quantitative model for EPISTAR perfusion imaging (abstr). In: Proceedings of the Third Meeting of the International Society for Magnetic Resonance in Medicine. Berkeley, Calif: International Society for Magnetic Resonance in Medicine, 1995; 132.
17. Wong EC, Frank LR, Buxton RB. Quantitative multislice perfusion imaging using QUIPSS II, EPISTAR, FAIR and PICORE (abstr). In: Proceedings of the Fifth Meeting of the International Society for Magnetic Resonance in Medicine. Berkeley, Calif: International Society for Magnetic Resonance in Medicine, 1997; 85.
18. Wolff SD, Balaban RS. Magnetization transfer contrast (MTC) and tissue water proton relaxation in vivo. Magn Reson Med 1989; 10:135–144.
19. Silva AC, Zhang W, Williams DS, Koretsky AP. Multislice MRI of rat brain perfusion during amphetamine stimulation using arterial spin labeling. Magn Reson Med 1995; 33:209–214.
20. Alsop DC. Correction of ghost artifacts and distortion in echo-planar MR imaging with an iterative image reconstruction technique (abstr.) Radiology 1995; 197(P):388.
21. Alsop DC, Detre JA. Reduction of excess noise in fMRI using noise image templates (abstr). In: Proceedings of the Fifth Meeting of the International Society for Magnetic Resonance in Medicine. Berkeley, Calif: International Society for Magnetic Resonance in Medicine, 1997; 1687.
22. Henkelman RM, Huang X, Xiang QS, Stanisz GJ, Swanson SD, Bronskill MJ. Quantitative interpretation of magnetization transfer. Magn Reson Med 1993; 29: 759–766.
23. Morrison C, Henkelman RM. A model for magnetization transfer in tissues. Magn Reson Med 1995; 33:475–482.
24. Maccotta L, Detre JA, Alsop DC. The efficiency of adiabatic inversion for perfusion imaging by arterial spin labeling. NMR Biomed 1997; 10:216–221.
25. Herscovitch P, Raichle ME. What is the correct value for the brain-blood partition coefficient for water. J Cereb Blood Flow Metab 1985; 5:65–69.
26. Ye FQ, Pekar JJ, Jezzard P, Duyn J, Frank JA, McLaughlin AC. Perfusion imaging of the human brain at 1.5 T using a single-shot EPI spin tagging approach. Magn Reson Med 1996; 36:217–224.
27. Matthew E, Andreason P, Carson RE, et al. Reproducibility of resting cerebral blood flow measurements with $H_2{}^{15}O$ positron emission tomography in humans. J Cereb Blood Flow Metab 1993; 13:748–754.
28. Pekar J, Jezzard P, Roberts DA, Leigh JS, Frank JA, McLaughlin AC. Perfusion imaging with compensation for asymmetric magnetization transfer effects. Magn Reson Med 1996; 35:70–79.
29. McKinnon GC. Ultrafast interleaved gradient echo planar imaging on a standard scanner. Magn Reson Med 1993; 30:609–616.
30. Hennig J, Nauerth A, Friedburg H. RARE imaging: a fast imaging method for clinical MR. Magn Reson Med 1986; 3:823–833.
31. Walsh EG, Minematsu K, Leppo J, Moore SC. Radioactive microsphere validation of a volume localized continuous saturation perfusion measurement. Magn Reson Med 1994; 31:147–153.
32. Detre JA, Alsop DC, Vives LR, Maccotta L, Teener JW, Raps EC. Noninvasive MRI evaluation of cerebral blood flow in cerebrovascular disease. Neurology 1998; 50: 633–641.